

Coordinating Self-Assembly of Copper Perylenetetracarboxylate Nanorods: Selectively Lighting up Normal Cells around Cancerous Ones for Better Cancer Diagnosis

Lizhi Wang,[†] Xuedong Gao,[‡] Ying Wei,[‡] Kaerdun Liu,[‡] Jianbin Huang,[‡] Jide Wang,^{*,†,‡} and Yun Yan^{*,‡,‡}

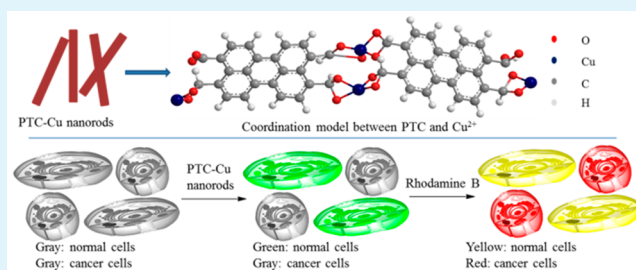
[†]Key Laboratory of Oil and Gas Fine Chemicals, Ministry of Education and Xinjiang Uygur Autonomous Region, College of Chemistry and Chemical Engineering, Xinjiang University, Urumqi 830046, People's Republic of China

[‡]Beijing National Laboratory for Molecular Sciences (BNLMS), State Key Laboratory for Structural Chemistry of Unstable and Stable Species, College of Chemistry and Molecular Engineering, Peking University, Beijing 100871, People's Republic of China

Supporting Information

ABSTRACT: Specific imaging of cancer cells has been well-accepted in cancer diagnosis although it cannot precisely mark the boundary between the normal and cancerous cells and report their mutual influence. We report a nanorod fluorescent probe of copper perylenetetracarboxylate (PTC-Cu) that can specifically light up normal cells. In combination with cancer cell imaging, the cocultured normal and cancer cells can be lit up with different colors, offering a clear contrast between the normal and cancer cells when they coexist. Because cancerous cells are only 20–30% in cancer area, this provides a possibility to visibly detect the mutual influence between the cancer and normal cells during therapy. We expect this method is beneficial to better cancer diagnosis and therapy.

KEYWORDS: Perylenetetracarboxylate, coordination, self-assembly, nanorods, fluorescent probe, selective stain, cell imaging



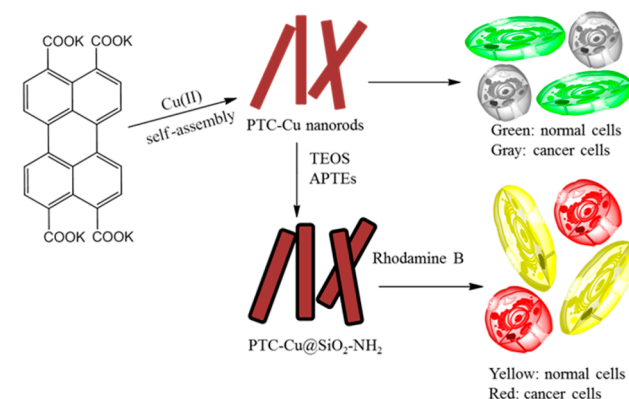
1. INTRODUCTION

Fluorescence imaging has emerged as a promising approach for diagnosis of diseases that threaten people's health.^{1–5} Compared with traditional clinically available imaging methods, such as positron emission tomography (PET),^{6–8} computed tomography (CT),^{9–11} and magnetic resonance imaging (MRI),¹² fluorescence imaging is advantageous for its high sensitivity, low-cost, low toxicity, and good accessibility.¹³ Therefore, diversified fluorescent dyes such as porphyrin,^{14–17} perylene,^{18–21} and rhodamine^{22–25} have been developed for cell and tissue imaging. Among these fluorescent dyes, perylene derivatives have attracted considerable interest because of their high molar absorptivity, high fluorescence quantum yields, and prominent thermal and photochemical stability.^{18–21,26,27} To achieve better specificity toward cancer cells, perylene-based molecules or nanoparticles are usually conjugated with tumor-specific biomarkers, such as peptides^{28–31} and antibodies.^{32–35} Although conjugation of biomolecules to fluorescent dyes can improve the imaging contrast between cancer and normal cells, this method involves complicated molecular design, tedious synthesis, and product purification procedure. Thus, it would be more fascinating if a fluorescent probe can be developed facilely with low cost.

An eternal issue in cell imaging for cancer therapy is to clearly mark the boundary between the healthy and diseased area, which are beneficial to precise cancer therapy.³⁶ Selectively staining cancer cells over normal ones is the mostly adopted idea for

effective diagnosis of cancers. Extraordinary works have been reported by Tang,^{1,3,37} Liu,³⁸ and Wolfbeis³⁹ et al. in recent decades. However, these imaging results tell little about the development and growth of normal cells around the cancerous area, so that it can hardly outline the real boundary between the normal and cancerous area precisely. Furthermore, the

Scheme 1. Design Strategy of the Fluorescent Probe for Tumor-Specific Imaging



Received: February 24, 2018

Accepted: May 7, 2018

Published: May 7, 2018

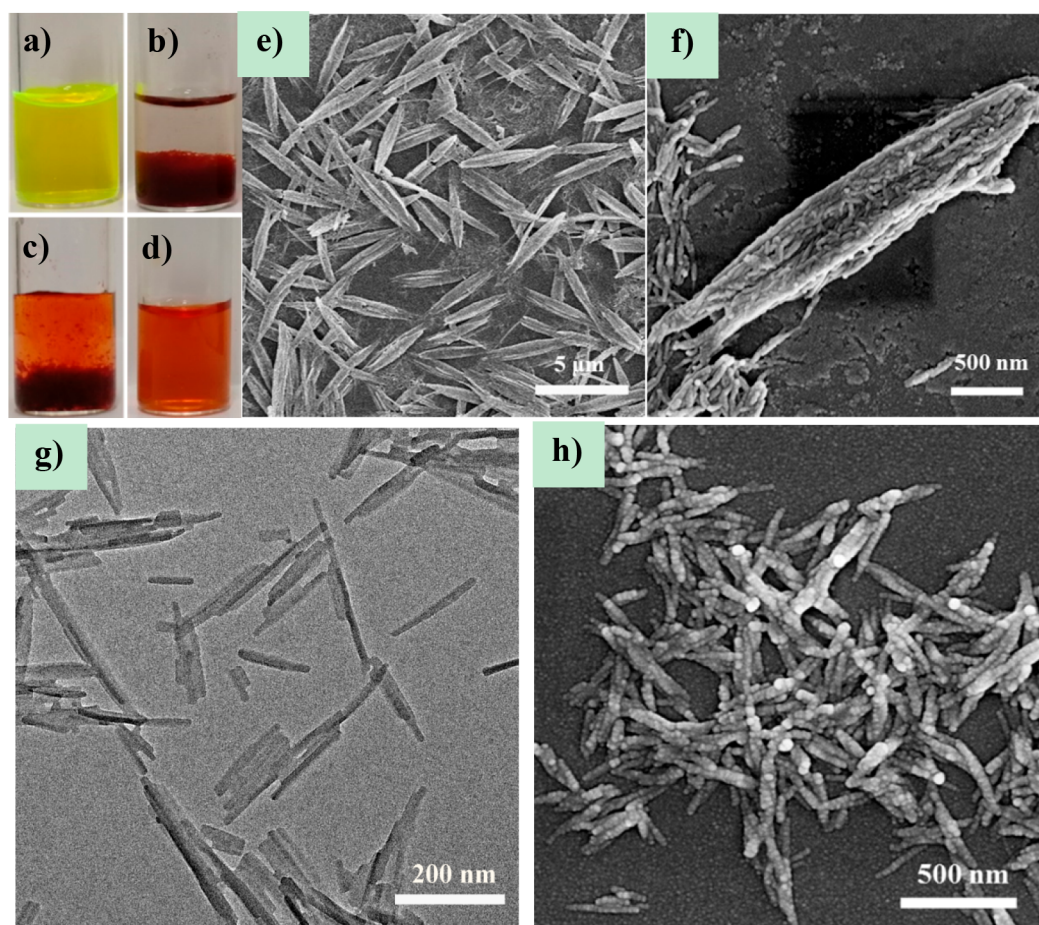


Figure 1. (a) The photo of the 2 mM K_4PTC water solution. (b) The photo of the red precipitates generated by addition of $Cu(NO_3)_2$ into the water solution of K_4PTC . (c) The red cloud produced by addition of water into the separated precipitates in b). (d) The red dispersion of the PTC-Cu nanorods in water. (e) SEM image of the PTC-Cu precipitates. (f) Enlarged SEM image of PTC-Cu precipitates. (g) TEM image of the PTC-Cu nanorods dispersed in water. (h) SEM image of the PTC-Cu nanorods.

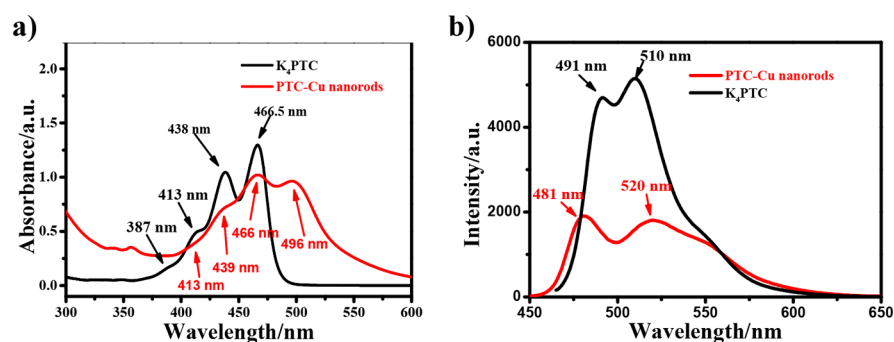


Figure 2. (a) UV-vis absorption spectra and (b) fluorescence spectrum of K_4PTC monomer (black line) and PTC-Cu nanorods (red line).

solely lighting-up of cancer cells cannot report the mutual influence between the cancer cells and the normal ones. Actually, the cancer cells is only 20–30% in a cancer tissue, whereas the others are all normal cells.^{40,41} Latest study shows that the presence of normal cells affects the efficiency of killing cancer cells.⁴² Therefore, selective staining of normal cells in the periphery of cancerous ones may offer valuable information about the mutual influence between cancer and normal cells. Especially, imaging the cancer cells and the normal ones with different colors will offer a very clear contrast between them, which allows a better understanding about the progress of the disease and help to make a precise outline of the development

of cancer. Therefore, fluorescent probes that are able to specifically light up normal cells are of significant importance for a better diagnosis and surgery treatment for cancers.

Herein we describe a new nanorod fluorescent probe constructed by the coordinating self-assembly of copper perylene-tetracarboxylate nanorods (PTC-Cu nanorods). This nanorod probe is facily prepared by mixing the aqueous solution of $Cu(NO_3)_2$ and potassium perylene-tetracarboxylate (K_4PTC). Suspension of PTC-Cu nanorods is obtained by washing the resultant bulk precipitates. The PTC-Cu nanorods have good biocompatibility and excellent selectivity toward normal cells in the presence of the cancerous ones. After coated by a layer of

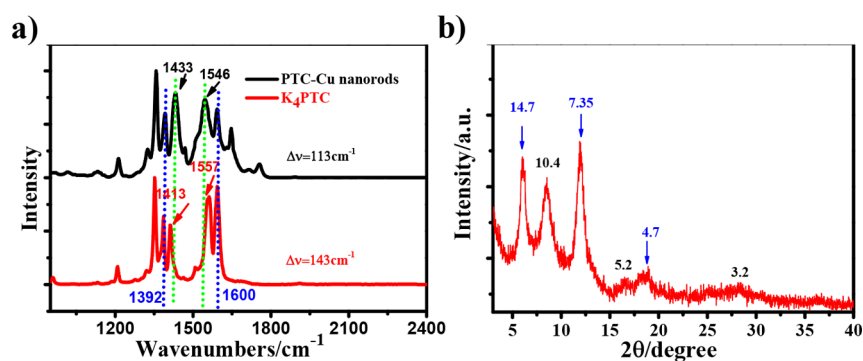
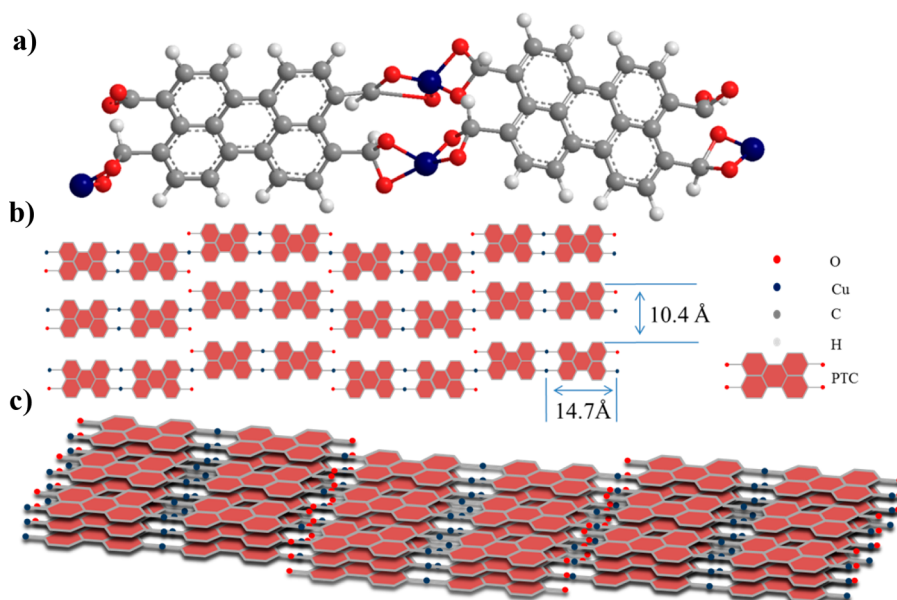


Figure 3. (a) FT-IR spectra of K_4 PTC (red line) and PTC-Cu nanorods (black line). (b) XRD patterns of the PTC-Cu nanorods in powder state (the unit of inserted distances is Å)

Scheme 2. Structures and Molecular Arrangements^a



^a(a) Ball and stick structure of the coordination between PTC and Cu^{2+} obtained from ChemBio3D ultra. (b,c) The molecular arrangement in the PTC-Cu nanorods in single layer and in three-dimensional space, respectively.

silica dioxide tagged with NH_2 group, the resultant PTC-Cu@ SiO_2-NH_2 nanorods display higher imaging contrast between normal and cancer cells. Most importantly, with the assistance of none selective staining dye of Rhodamine B, the cancer cells and the normal cells can be illuminated by different colors (Scheme 1). Compared to diagnosis based on solely lighting-up cancer cells, illuminating the periphery normal cells around the cancerous ones with a different color allows a better understanding of the status of the disease area both before and in the process of treatment. We expect that selective staining of normal cells may add additional option to enhanced cancer diagnosis and therapy.

2. RESULTS AND DISCUSSION

The self-assembled system is based on the potassium salt of 3,4,9,10-perylenetetracarboxylate (K_4 PTC) and $Cu(NO_3)_2$. K_4 PTC forms a transparent yellow-green solution in water at the concentration of 2 mM (Figure 1a). Upon addition of aqueous solution of $Cu(NO_3)_2$ at the molar ratio of PTC: Cu^{2+} = 1:2, red precipitates occur immediately (Figure 1b), suggesting coordination has occurred between Cu^{2+} and the carboxylate group of PTC. Just like other metal coordinated

with PTC in the literature,^{43–45} the precipitates of PTC-Cu are spindle rods with average lengths of 5–7 μm and widths of 400–600 nm (Figure 1e, Figure S1a–c). Enlarged SEM image reveals that the micrometer sized spindle rods are composed of nanorods (Figure 1f). Interestingly, the nanorods can be released from the precipitates upon washing the separated precipitates with water. Figure 1c shows that red cloud arises from the bulk precipitates, which is able to form homogeneous colloidal suspension after slight shaking. This red colloidal suspension remains stable for weeks after separated from the bulk precipitates (Figure 1d), and are stable for months when stored in ethanol. Red powders can be obtained upon evaporation of ethanol, but the powder can be easily dispersed into pure water to form red dispersion again. TEM (Figure 1g and S 1d) and SEM (Figure 1h) measurements confirms that the colloidal particle in the red dispersion are nanorods of 10–20 nm wide and 100–200 nm long.

Figure 2a shows the UV–vis spectra of PTC-Cu nanorods and K_4 PTC in aqueous solution. The absorption spectrum of dilute K_4 PTC solution displays four peaks including two pronounced peaks at 466.5 and 438 nm, and two shoulders at 413 and 387 nm, corresponding to the 0–0, 0–1, 0–2 and 0–3

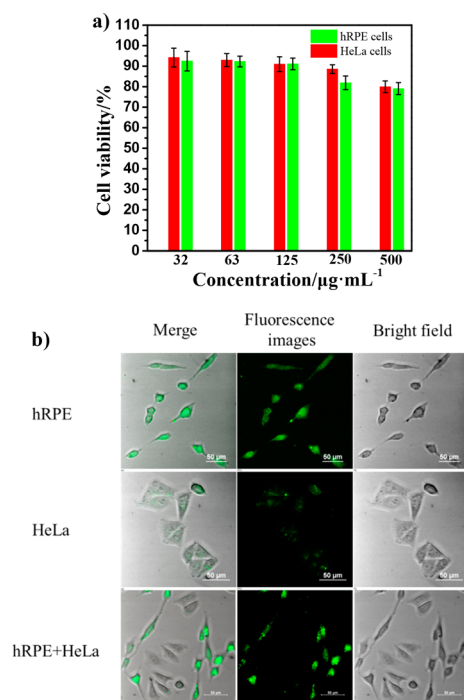


Figure 4. (a) Cytotoxicity of PTC-Cu nanorods toward HeLa and hRPE cells (incubate for 24 h). (b) CLSM images of HeLa cells, hRPE cells, and coincubated with PTC-Cu nanorods for 12 h (λ_{ex} 488 nm; λ_{em} 500–530 nm). Scale bar: 50 μm .

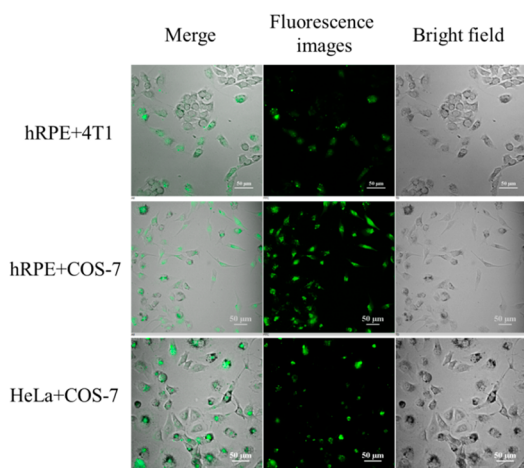


Figure 5. CLSM images of cells coincubated: hRPE and 4T1 cells, hRPE and COS-7 cells, and HeLa and COS-7 cells (incubated with PTC-Cu nanorods for 12 h, λ_{ex} 488 nm; λ_{em} 500–530 nm).

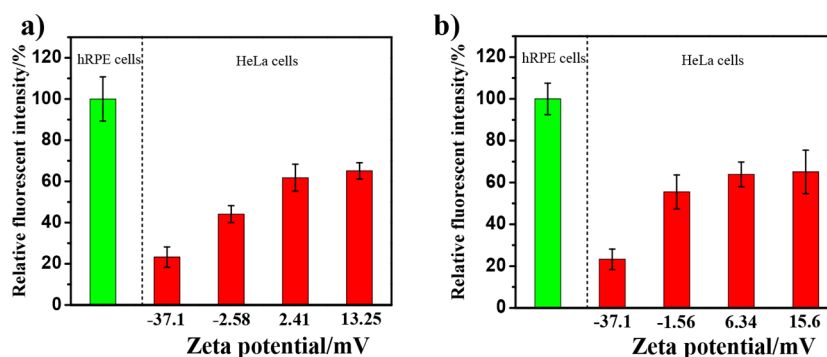


Figure 6. Relative fluorescent intensity of cells stained with (a) PTC-Cu@PG₁₂-b-PEO₂₀₅-b-PG₁₂ and (b) PTC-Cu@PLL.

electronic transitions, respectively.⁴⁶ However, the UV–vis spectrum for the PTC-Cu nanorods is drastically broadened and red-shifted to 496, 466, 439, and 412 nm, suggesting the electronic states of PTC skeleton have been changed in the PTC-Cu nanorods. In line with the changes of UV–vis absorbance, the fluorescence emission of the PTC-Cu nanorods is also different from that of the K₄PTC aqueous solution. Except broadening and bathochromic shift of the emission peaks, the shoulder emission corresponding to the excimers becomes pronounced, indicating the interaction between PTC skeletons is very significant.^{47,48}

Elemental analysis from ultraviolet spectrophotometry and ICP-AES of the nanorod suggests that the molar ratio of PTC and Cu²⁺ is 2:3, which differs from the mixing ratio of 1:2 in the original solution. Since one would expect the 1:2 ratio for PTC/Cu²⁺ in a saturate coordination and the ratio of 1:1 for a half saturate coordination, the present results indicates the nanorods are composed of PTC and Cu²⁺ in the coordinating state of PTC-Cu²⁺ and PTC-2Cu²⁺ half-to-half. Fourier transform-infrared (FT-IR) measurements (Figure 3a) confirm the presence of two coordinating states of PTC in the nanorods. It can be read from Figure 3a that the vibrational bands of uncoordinated COO⁻ at 1600 and 1392 cm⁻¹ is copresent with the coordinated COO⁻ at 1546 and 1433 cm⁻¹.^{43,44,49,50}

In order to have better physical insight about the molecular packing in the nanorods, X-ray diffraction (XRD) measurements were performed. Two sets of peaks featuring lamellar structures are observed in the XRD patterns for the nanorods. One set occurs at $2\theta = 6.0^\circ$, 12.0° , and 18.0° , corresponding to distance of 14.7, 7.35, and 4.7 Å, respectively; and the other set occurs at $2\theta = 8.4^\circ$, 16.8° with $d = 10.4$, 5.2 Å, as indicated in Figure 3b. The d value of 14.7 Å is close to the length of the cooper coordinated PTC skeleton coordinated with Cu²⁺, namely, the length of the PTC skeleton with the length of Cu–O coordination bond according to molecular modeling. Interestingly, the distance of 10.5 Å is close to the 1.5 folds of the width of the PTC skeleton. This indicates the saturate and half-saturate coordinating states have arranged alternatively with a dislocation, as illustrated in Scheme 2a–c. It is noticed that a weak, broaden peak occurs at $2\theta = 28^\circ$ corresponding to d value of 3.2 Å, suggesting that the dislocated PTC-Cu²⁺ layers have staked into layered structures via π – π stacking between the PTC skeletons⁵¹ but this stacking is not very significant due to the presence of dislocation, and the repulsive forces originated from the uncoordinated COO⁻ groups. This agrees well with the retained fluorescence of PTC, because perfect π – π stacking will cause notorious fluorescence quenching.

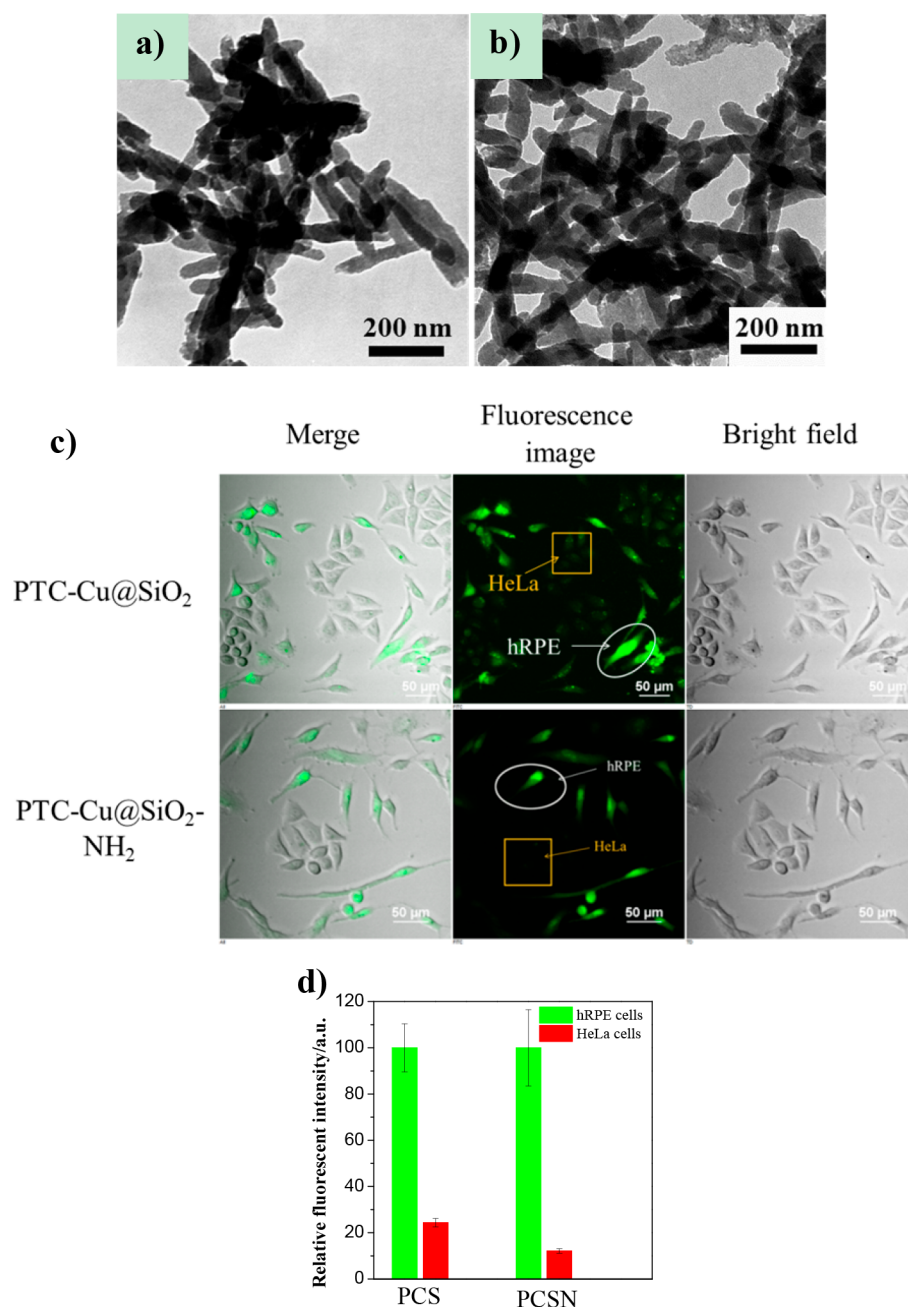


Figure 7. (a) TEM image of PTC-Cu@SiO₂ nanorods. (b) TEM image of PTC-Cu@SiO₂-NH₂ nanorods. (c) CLSM images of HeLa and hRPE cells coincubated with PTC-Cu@SiO₂ nanorods and PTC-Cu@SiO₂-NH₂ nanorods for 12 h. (λ_{ex} 488 nm; λ_{em} 500–530 nm). (d) Relative fluorescent intensity of the hRPE and HeLa cells with PTC-Cu@SiO₂ nanorods and PTC-Cu@SiO₂-NH₂ nanorods obtained from statistical analysis of the CLSM images in (c). PCS represents the nanorods of PTC-Cu@SiO₂, and PCSN represents that of PTC-Cu@SiO₂-NH₂.

The sufficient fluorescence and the sufficiently small size of the PTC-Cu nanorods provides a possibility for using them as fluorescent probes in cell imaging. Then the cytotoxicity of PTC-Cu nanorods toward HeLa and hRPE cells were evaluated using the 3-(4,5-dimethyl-2-thiazolyl)-2,5-diphenyltetrazolium bromide (MTT) assay. As shown in Figure 4a, the PTC-Cu nanorods do not exhibit obvious cytotoxicity to HeLa and hRPE cells even when their concentrations are as high as 500 $\mu\text{g}\cdot\text{mL}^{-1}$. This bodes well for the utility of this fluorescent probe, particularly in living cell imaging applications.

Living cell imaging based on PTC-Cu nanorods was investigated with confocal laser scanning microscope (CLSM). Cervical cancer HeLa and hRPE cells were incubated with 125 $\mu\text{g}\cdot\text{mL}^{-1}$

PTC-Cu nanorods for 12 h, and excess nanorods were washed away with PBS buffer. Interestingly, the healthy hRPE cells are illuminated, whereas the cancerous HeLa cells remain dark (Figure 4b). Quantitative analysis suggests the fluorescence intensity in the HeLa cell is only about 22% of that in the hRPE cells. When the two cells are cocultured together, the fluorescence from the HeLa cells is negligible, verifying that the PTC-Cu nanorods are able to selectively light up the hRPE cells.

To explore whether the PTC-Cu nanorods could be used as a selective fluorescent probe for other cells, two more cell lines, one that is the cancerous cell of 4T1 cells and the other that is the normal cell of COS-7, were stained with PTC-Cu nanorods. Figure 5 reveals the normal COS-7 cells can be lit up by the

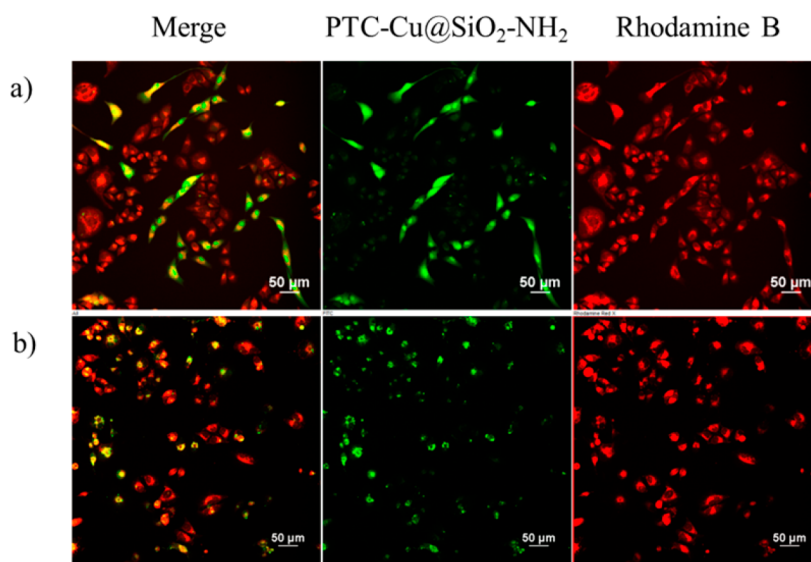


Figure 8. Coculture of different combinations of cancer and normal cells in culture medium containing the PTC-Cu@SiO₂-NH₂ nanorods (λ_{ex} , 488 nm; λ_{em} , 500–530 nm) and Rhodamine B for 12h (λ_{ex} , 543 nm; λ_{em} , 552–617 nm). (a) HeLa and hRPE cells. (b) HeLa and COS-7 cells.

PTC-Cu nanorods as well, whereas the cancerous cells of 4T1 remain dark when they are cocultured with the normal hRPE and COS-7 cells, demonstrating that the PTC-Cu nanorods can preferentially light up normal cells in the presence cancerous ones. This allows using the PTC-Cu nanorods as potentially effective fluorescent probe for specific staining of normal cells.

The selective staining ability of the PTC-Cu nanorods toward normal cells, rather than the cancerous ones, is rather amazing because cancer cells usually have better ability to uptake various nanoparticles via endocytosis due to their looser membrane structure.^{52–54} In order to have a better understanding about this abnormal selectivity, the effect of aspect ratio and surface charge of the PTC-Cu nanorods on cell staining were studied, respectively. First of all, the impact of aspect ratio of PTC-Cu nanorods was tested. In literature reports, aspect ratio of nanoparticles has a significant effect on the endocytosis behavior.^{55–58} For instance, the cellular uptake efficiency of untargeted gold nanoparticles monotonically decreases with aspect ratios.⁵⁵ However, as the aspect ratio of the PTC-Cu nanorods is varied between 4 and 9 (Figure S2), no detectable difference in the cell selectivity is observed (Figure S3), suggesting the change in aspect ratio in the present study is not sensitive to the selective cell staining behavior.

Next, the impact of the surface charge of the PTC-Cu nanorods on the selective behavior was examined. PTC-Cu nanorods have a negative surface potential of -37.1 mV. As the PTC-Cu nanorods were rapped with a layer of PG₁₂-*b*-PEO₂₀₅-*b*-PG₁₂ (Figure S4a,b) or ϵ -polylysine (ϵ -PLL, Figure S5a,b), their surface potential becomes nearly zero or reverses to a small positive value. Surprisingly, these rapped PTC-Cu nanorods lose the ability of selectively staining any kind of cells (Figures S4c and 5c). Both the normal and the cancerous ones were illuminated after incubating with PTC-Cu nanorods, suggesting the surface of the PTC-Cu nanorods has great impact on their ability of selective cell staining (Figure 6a,b).

However, as we coated the surface of the PTC-Cu nanorods with a layer of SiO₂, they still selectively stain the normal cells. Figure 7a,b shows that after introducing either tetraethoxysilane (TEOS) or (3-aminopropyl)triethoxysilane (APTEs) to the suspension of PTC-Cu nanorods, a layer of silica was deposited

onto the surface of PTC-Cu nanorods. The resultant nanorods are denoted as PTC-Cu@SiO₂ and PTC-Cu@SiO₂-NH₂, respectively. Energy dispersive X-ray (EDX) measurement (Figure S6) verifies the presence of Si and O in the nanorods, and their molar ratio is about 1:2. Meanwhile, the characteristic strong asymmetric vibration of Si—O—Si at 1060–1150 cm⁻¹ and symmetric vibration of SiO₄ network at 805 cm⁻¹ are observed in FT-IR spectra (Figure S7), suggesting the successful coating of SiO₂ on the surface of the PTC-Cu nanorods.⁵⁹ The zeta potential for the PTC-Cu@SiO₂ nanorods and PTC-Cu@SiO₂-NH₂ nanorods is -17.3 mV and 24.8 mV, respectively. However, both the negatively charged PTC-Cu@SiO₂ nanorods and the positively charged PTC-Cu@SiO₂-NH₂ nanorods can selectively stain hRPE cells (Figure 7c). Figure 7d shows the fluorescence intensity of HeLa and hRPE cells stained with the PTC-Cu@SiO₂ nanorods and PTC-Cu@SiO₂-NH₂ nanorods, respectively. The selectivity of PTC-Cu@SiO₂ nanorods toward normal cells is similar to that of the naked PTC-Cu nanorods, as revealed by the similar level of fluorescence intensity of HeLa (24.4% of the intensity for hRPE cells). However, the background fluorescence of HeLa cells is sharply decreased to 12.1% in the PTC-Cu@SiO₂-NH₂ nanorods system, indicating an enhanced selectivity toward normal cells. It is rather amazing that the positive surface of the PTC-Cu@SiO₂-NH₂ nanorods still displays unique selectivity toward normal cells, as most positively charged molecular dyes prefer to stain cancer cells.^{37,60,61} This means that the surface component of nanoparticles has an even stronger impact on their ability of endocytosis. In a control experiment, we found that the single solution of K₄PTC can also selectively stain normal cells (Figure S8a) but the background contrast is as high as 52% (Figure S8b). We postulate it is possible that the surface component of a normal cell can specifically interact with the PTC skeleton, so that the PTC-Cu nanorods display specific recognition to normal cells.

The strong preference of the PTC-Cu nanorods toward normal cells offers a possibility to mark the boundary between the normal and cancerous cells by staining both of them. Because the PTC-Cu@SiO₂-NH₂ nanorods have the best selectivity efficiency to hRPE cells, they are used as fluorescent probe to mark the boundary between cancer and normal cells. Because

cancer cells cannot be illuminated by PTC-Cu@SiO₂-NH₂ nanorods directly, Rhodamine B was introduced to our system. As shown in Figure 8a, both hRPE and HeLa cells are illuminated by Rhodamine B, while only hRPE cells are illuminated by the PTC-Cu@SiO₂-NH₂ nanorods. Therefore, in the merged image the hRPE cells are yellow while the HeLa cells are red. As for HeLa and COS-7 cells, the same results are obtained (Figure 8b). The high imaging contrast between the cancer and normal cells makes it possible to see the status of the normal cells among the cancerous ones. Because the cancer cells are only about 20–30% in a cancer tissue, whereas the other 70–80% are all normal ones,^{40,41} the coilluminating strategy allows us to have a better understanding about the mutual influence of the cancerous and the normal cells during a therapy. Indeed, recent study reveals that the treatment of cancer will be influenced by the presence of normal cells.^{40,41} We expect that the present work not only aids to mark a precise boundary between the cancerous and the normal cells but also help to provide more physical insight in cancer therapy.

3. CONCLUSION

In summary, a nanorod fluorescence probe PTC-Cu that is able to specifically stain normal cells, such as hRPE and COS-7 cells, was developed. Surface coating of the nanorods with NH₂ tag can enhance the selectivity toward normal cells. In combination with cancerous cell imaging, this normal cell staining probe allows lighting-up both the cancer cells and its periphery normal cells with different colors. We find the surface group plays much important role than electrical charges in selectively staining cells. We expect that the strategy of lighting-up both the cancer cells and the normal ones in their periphery helps to mark a clearer boundary between them, which offers a better diagnostic and treatment to cancers.

■ ASSOCIATED CONTENT

Supporting Information

The Supporting Information is available free of charge on the ACS Publications website at DOI: 10.1021/acsami.8b03211.

Experimental section and supplemental figures. Experimental section includes materials, synthesis, and methods. Supplemental figures include TEM and SEM images of PTC-Cu precipitates (Figure S1), TEM images of PTC-Cu nanorods with different aspect ratios (Figure S2), CLSM images of HeLa and hRPE cells coincubated with PTC-Cu nanorods for different aspect ratios (Figure S3), CLSM images of HeLa and hRPE cells coincubated with PTC-Cu@PG₁₂-b-PEO₂₀₅-b-PG₁₂ for different surface charges for 12 h (Figure S4), CLSM images of HeLa and hRPE cells coincubated with PTC-Cu@PLL for different surface charges for 12 h (Figure S5), EDX measurement of PTC-Cu nanorods (Figure S6), FT-IR spectrum of PTC-Cu nanorods (blue line), PTC-Cu@SiO₂ nanorods (black line) and PTC-Cu@SiO₂-NH₂ nanorods (red line) (Figure S7), CLSM images of HeLa and hRPE cells coincubated with K₄PTC for 12 h (Figure S8) (PDF)

■ AUTHOR INFORMATION

Corresponding Authors

*(Y.Y.) E-mail: yunyan@pku.edu.cn.

*(J.W.) E-mail: awangjd@sina.cn.

ORCID

Jide Wang: 0000-0002-7740-9408

Yun Yan: 0000-0001-8759-3918

Notes

The authors declare no competing financial interest.

■ ACKNOWLEDGMENTS

Authors are grateful to National Natural Science Foundation of China (Grants 21573011 and 21422302) and the Beijing National Laboratory for Molecular Sciences (BNLMS) for financial support.

■ REFERENCES

- (1) Qian, J.; Tang, B. Z. AIE Luminogens for Bioimaging and Theranostics: From Organelles to Animals. *Chem.* **2017**, *3* (1), S6–91.
- (2) Yang, Y.; Zhao, Q.; Feng, W.; Li, F. Luminescent Chemodosimeters for Bioimaging. *Chem. Rev.* **2013**, *113* (1), 192–270.
- (3) Liang, J.; Tang, B. Z.; Liu, B. Specific Light-up Bioprobes Based on AIEgen Conjugates. *Chem. Soc. Rev.* **2015**, *44* (10), 2798–2811.
- (4) Kwok, R. T.; Leung, C. W.; Lam, J. W.; Tang, B. Z. Biosensing by Luminogens with Aggregation-Induced Emission Characteristics. *Chem. Soc. Rev.* **2015**, *44* (13), 4228–4238.
- (5) Kobayashi, H.; Ogawa, M.; Alford, R.; Choyke, P. L.; Urano, Y. New Strategies for Fluorescent Probe Design in Medical Diagnostic Imaging. *Chem. Rev.* **2010**, *110* (5), 2620–2640.
- (6) Perera, M.; Papa, N.; Christidis, D.; Wetherell, D.; Hofman, M. S.; Murphy, D. G.; Bolton, D.; Lawrentschuk, N. Sensitivity, Specificity, and Predictors of Positive (68)Ga-Prostate-specific Membrane Antigen Positron Emission Tomography in Advanced Prostate Cancer: A Systematic Review and Meta-analysis. *Eur. Urol.* **2016**, *70* (6), 926–937.
- (7) André, M. P. E.; Girinsky, T.; Federico, M.; Reman, O.; Fortpied, C.; Gotti, M.; Casasnovas, O.; Brice, P.; van der Maazen, R.; Re, A.; Edeline, V.; Fermé, C.; van Imhoff, G.; Merli, F.; Bouabdallah, R.; Sebban, C.; Specht, L.; Stamatoullas, A.; Delarue, R.; Fiaccadori, V.; Bellei, M.; Raveloarivahy, T.; Versari, A.; Hutchings, M.; Meignan, M.; Raemaekers, J. Early Positron Emission Tomography Response-Adapted Treatment in Stage I and II Hodgkin Lymphoma: Final Results of the Randomized EORTC/LYSA/FIL H10 Trial. *J. Clin. Oncol.* **2017**, *35* (16), 1786–1794.
- (8) Hwang, D.; Jeon, K. H.; Lee, J. M.; Park, J.; Kim, C. H.; Tong, Y.; Zhang, J.; Bang, J. I.; Suh, M.; Paeng, J. C.; Na, S. H.; Cheon, G. J.; Cook, C. M.; Davies, J. E.; Koo, B. K. Diagnostic Performance of Resting and Hyperemic Invasive Physiological Indices to Define Myocardial Ischemia: Validation With (13)N-Ammonia Positron Emission Tomography. *JACC Cardiovasc. Interv.* **2017**, *10* (8), 751–760.
- (9) Kalender, W. A. X-ray Computed Tomography. *Phys. Med. Biol.* **2006**, *51* (13), R29–43.
- (10) van Rosendaal, P. J.; Kamperidis, V.; Kong, W. K.; van Rosendaal, A. R.; van der Kley, F.; Ajmone Marsan, N.; Delgado, V.; Bax, J. J. Computed Tomography for Planning Transcatheter Tricuspid Valve Therapy. *Eur. Heart J.* **2016**, *38* (9), ehv499.
- (11) Leipsic, J.; Abbara, S.; Achenbach, S.; Cury, R.; Earls, J. P.; Mancini, G. J.; Nieman, K.; Pontone, G.; Raff, G. L. SCCT Guidelines for the Interpretation and Reporting of Coronary CT Angiography: a Report of the Society of Cardiovascular Computed Tomography Guidelines Committee. *J. Cardiovasc. Comput. Tomogr.* **2014**, *8* (5), 342–358.
- (12) Huang, P.; Qian, X.; Chen, Y.; Yu, L.; Lin, H.; Wang, L.; Zhu, Y.; Shi, J. Metalloporphyrin-Encapsulated Biodegradable Nanosystems for Highly Efficient Magnetic Resonance Imaging-Guided Sonodynamic Cancer Therapy. *J. Am. Chem. Soc.* **2017**, *139* (3), 1275–1284.
- (13) Liu, J. N.; Bu, W.; Shi, J. Chemical Design and Synthesis of Functionalized Probes for Imaging and Treating Tumor Hypoxia. *Chem. Rev.* **2017**, *117* (9), 6160–6224.
- (14) Mauriello-Jimenez, C.; Henry, M.; Aggad, D.; Raehm, L.; Cattoen, X.; Wong Chi Man, M.; Charnay, C.; Alpugan, S.; Ahsen, V.; Tarakci, D. K.; Maillard, P.; Maynadier, M.; Garcia, M.; Dumoulin, F.;

- Gary-Bobo, M.; Coll, J. L.; Josserand, V.; Durand, J. O. Porphyrin- or Phthalocyanine-Bridged Silsesquioxane Nanoparticles for Two-Photon Photodynamic Therapy or Photoacoustic Imaging. *Nanoscale* **2017**, *9* (43), 16622–16626.
- (15) Bhattarai, P.; Liang, X.; Xu, Y.; Dai, Z. A Novel Cyanine and Porphyrin Based Theranostic Nanoagent for Near-Infrared Fluorescence Imaging Guided Synergistic Phototherapy. *J. Biomed. Nanotechnol.* **2017**, *13* (11), 1468–1479.
- (16) Liu, K.; Xing, R.; Zou, Q.; Ma, G.; Mohwald, H.; Yan, X. Simple Peptide-Tuned Self-Assembly of Photosensitizers towards Anticancer Photodynamic Therapy. *Angew. Chem., Int. Ed.* **2016**, *55* (9), 3036–3039.
- (17) Zhang, T.; Chan, C. F.; Lan, R.; Li, H.; Mak, N. K.; Wong, W. K.; Wong, K. L. Porphyrin-Based Ytterbium Complexes Targeting Anionic Phospholipid Membranes as Selective Biomarkers for Cancer Cell Imaging. *Chem. Commun. (Cambridge, U. K.)* **2013**, *49* (65), 7252–7254.
- (18) Xu, Z.; Guo, K.; Yu, J.; Sun, H.; Tang, J.; Shen, J.; Mullen, K.; Yang, W.; Yin, M. A Unique Perylene-Based DNA Intercalator: Localization in Cell Nuclei and Inhibition of Cancer Cells and Tumors. *Small* **2014**, *10* (20), 4087–4092.
- (19) Muthuraj, B.; Mukherjee, S.; Chowdhury, S. R.; Patra, C. R.; Iyer, P. K. An Efficient Strategy to Assemble Water Soluble Histidine-Perylene Diimide and Graphene Oxide for the Detection of PPI in Physiological Conditions and in Vitro. *Biosens. Bioelectron.* **2017**, *89*, 636–644.
- (20) Jana, A.; Devi, K. S.; Maiti, T. K.; Singh, N. D. Perylene-3-ylmethanol: Fluorescent Organic Nanoparticles as a Single-Component Photoresponsive Nanocarrier with Real-Time Monitoring of Anticancer Drug Release. *J. Am. Chem. Soc.* **2012**, *134* (18), 7656–7659.
- (21) Gao, B.; Li, H.; Liu, H.; Zhang, L.; Bai, Q.; Ba, X. Water-Soluble and Fluorescent Dendritic Perylene Bisimides for Live-Cell Imaging. *Chem. Commun. (Cambridge, U. K.)* **2011**, *47* (13), 3894–3896.
- (22) Lavis, L. D. Teaching Old Dyes New Tricks: Biological Probes Built from Fluoresceins and Rhodamines. *Annu. Rev. Biochem.* **2017**, *86*, 825–843.
- (23) Butkevich, A. N.; Mitronova, G. Y.; Sidenstein, S. C.; Klocke, J. L.; Kamin, D.; Meineke, D. N.; D'Este, E.; Kraemer, P. T.; Danzl, J. G.; Belov, V. N.; et al. Fluorescent Rhodamines and Fluorogenic Carbopyronines for Super-Resolution STED Microscopy in Living Cells. *Angew. Chem., Int. Ed.* **2016**, *55* (10), 3290–3294.
- (24) Wysocki, L. M.; Grimm, J. B.; Tkachuk, A. N.; Brown, T. A.; Betzig, E.; Lavis, L. D. Facile and General Synthesis of Photoactivatable Xanthene Dyes. *Angew. Chem., Int. Ed.* **2011**, *50* (47), 11206–11209.
- (25) Li, K. B.; Wang, H.; Zang, Y.; He, X. P.; Li, J.; Chen, G. R.; Tian, H. One-Step Click Engineering Considerably Ameliorates the Practicality of an Unqualified Rhodamine Probe. *ACS Appl. Mater. Interfaces* **2014**, *6* (22), 19600–19605.
- (26) Chen, S.; Slattum, P.; Wang, C.; Zang, L. Self-Assembly of Perylene Imide Molecules into 1D Nanostructures: Methods, Morphologies, and Applications. *Chem. Rev.* **2015**, *115* (21), 11967–11998.
- (27) Blechinger, J.; Herrmann, R.; Kiener, D.; Garcia-Garcia, F. J.; Scheu, C.; Reller, A.; Brauchle, C. Perylene-Labeled Silica Nanoparticles: Synthesis and Characterization of Three Novel Silica Nanoparticle Species for Live-Cell Imaging. *Small* **2010**, *6* (21), 2427–2435.
- (28) Choi, H. S.; Gibbs, S. L.; Lee, J. H.; Kim, S. H.; Ashitate, Y.; Liu, F.; Hyun, H.; Park, G.; Xie, Y.; Bae, S.; Henary, M.; Frangioni, J. V. Targeted Zwitterionic Near-Infrared Fluorophores for Improved Optical Imaging. *Nat. Biotechnol.* **2013**, *31* (2), 148–153.
- (29) Morales, A. R.; Yanez, C. O.; Zhang, Y.; Wang, X.; Biswas, S.; Urakami, T.; Komatsu, M.; Belfield, K. D. Small Molecule Fluorophore and Copolymer RGD Peptide Conjugates for ex Vivo Two-Photon Fluorescence Tumor Vasculature Imaging. *Biomaterials* **2012**, *33* (33), 8477–8485.
- (30) Wang, H.; Zhang, Q.; Chu, X.; Chen, T.; Ge, J.; Yu, R. Graphene Oxide-Peptide Conjugate as an Intracellular Protease Sensor for Caspase-3 Activation Imaging in Live Cells. *Angew. Chem., Int. Ed.* **2011**, *50* (31), 7065–7069.
- (31) Lagunas, A.; Tsintzou, I.; Vida, Y.; Collado, D.; Pérez-Inestrosa, E.; Rodríguez Pereira, C.; Magalhaes, J.; Andrades, J. A.; Samitier, J. Tailoring RGD Local Surface Density at the Nanoscale Toward Adult Stem Cell Chondrogenic Commitment. *Nano Res.* **2017**, *10* (6), 1959–1971.
- (32) Xiong, K.; Wei, W.; Jin, Y.; Wang, S.; Zhao, D.; Wang, S.; Gao, X.; Qiao, C.; Yue, H.; Ma, G.; Xie, H. Y. Biomimetic Immuno-Magnetosomes for High-Performance Enrichment of Circulating Tumor Cells. *Adv. Mater.* **2016**, *28* (36), 7929–7935.
- (33) Wang, Y.; Zhou, K.; Huang, G.; Hensley, C.; Huang, X.; Ma, X.; Zhao, T.; Sumer, B. D.; DeBerardinis, R. J.; Gao, J. A Nanoparticle-Based Strategy for the Imaging of a Broad Range of Tumours by Nonlinear Amplification of Microenvironment Signals. *Nat. Mater.* **2014**, *13* (2), 204–212.
- (34) Mohamadi, R. M.; Besant, J. D.; Mephram, A.; Green, B.; Mahmoudian, L.; Gibbs, T.; Ivanov, I.; Malvea, A.; Stojic, J.; Allan, A. L.; Lowes, L. E.; Sargent, E. H.; Nam, R. K.; Kelley, S. O. Nanoparticle-Mediated Binning and Profiling of Heterogeneous Circulating Tumor Cell Subpopulations. *Angew. Chem., Int. Ed.* **2015**, *54* (1), 139–143.
- (35) Song, Y.; Zhu, Z.; An, Y.; Zhang, W.; Zhang, H.; Liu, D.; Yu, C.; Duan, W.; Yang, C. J. Selection of DNA Aptamers Against Epithelial Cell Adhesion Molecule for Cancer Cell Imaging and Circulating Tumor Cell Capture. *Anal. Chem.* **2013**, *85* (8), 4141–4149.
- (36) Whitley, M. J.; et al. A Mouse-Human Phase 1 Co-Clinical Trial of a Protease-Activated Fluorescent Probe for Imaging Cancer. *Sci. Transl. Med.* **2016**, *8* (320), 320ra4.
- (37) Gui, C.; Zhao, E.; Kwok, R. T. K.; Leung, A. C. S.; Lam, J. W. Y.; Jiang, M.; Deng, H.; Cai, Y.; Zhang, W.; Su, H.; Tang, B. Z. AIE-Active Theranostic System: Selective Staining and Killing of Cancer Cells. *Chem. Sci.* **2017**, *8* (3), 1822–1830.
- (38) Liu, B. Aggregation-Induced Emission: Materials and Biomedical Applications. *MRS Bull.* **2017**, *42* (06), 458–463.
- (39) Wolfbeis, O. S. An Overview of Nanoparticles Commonly Used in Fluorescent Bioimaging. *Chem. Soc. Rev.* **2015**, *44* (14), 4743–4768.
- (40) Flier, J. S.; et al. Tumors: Wounds That Do Not Heal. *N. Engl. J. Med.* **1986**, *315* (26), 1650–1659.
- (41) Balkwill, F.; Mantovani, A. Inflammation and Cancer: Back to Virchow? *Lancet* **2001**, *357* (9255), 539–545.
- (42) Chen, D.; Wang, H.; Liu, P.; Song, L.; Shi, J.; Tong, B.; Dong, Y. The Application of CO₂-Sensitive AIEgen in Studying the Synergistic Effect of Stromal Cells and Tumor Cells in a Heterocellular System. *Anal. Chim. Acta* **2018**, *1001*, 151–157.
- (43) Wang, Y.; Gao, X.; Xiao, Y.; Zhao, Q.; Yang, J.; Yan, Y.; Huang, J. Temperature Dependent Coordinating Self-Assembly. *Soft Matter* **2015**, *11* (14), 2806–2811.
- (44) Gao, X.; Wang, Y.; Wang, X.; Guo, X.; Huang, J.; Yan, Y. Concentration-Tailored Self-Assembly Composition and Function of the Coordinating Self-Assembly of Perylenetetracarboxylate. *J. Mater. Chem. C* **2017**, *5* (35), 8936–8943.
- (45) Bai, L.; Xia, Y.; Jana, A.; Ang, C. Y.; Zhao, L.; Fan, Z.; Zhao, Y. Perylenetetracarboxylic-Metal Assemblies and Anisotropic Charge Transport in a Cu(II) Assembly. *Nanoscale* **2016**, *8* (17), 9134–9140.
- (46) Wang, Y.; Gao, X.; Xiao, Y.; Zhao, Q.; Yang, J.; Yan, Y.; Huang, J. Temperature Dependent Coordinating Self-Assembly. *Soft Matter* **2015**, *11* (14), 2806–2811.
- (47) Huang, C.; Barlow, S.; Marder, S. R. Perylene-3,4,9,10-tetracarboxylic Acid Diimides: Synthesis, Physical Properties, and Use in Organic Electronics. *J. Org. Chem.* **2011**, *76* (8), 2386–2407.
- (48) Wei, Z.; Laitinen, T.; Smarsly, B.; Ikkala, O.; Faul, C. F. Self-Assembly and Electrical Conductivity Transitions in Conjugated Oligoaniline-Surfactant Complexes. *Angew. Chem., Int. Ed.* **2005**, *44* (5), 751–756.
- (49) Deacon, G.; Phillips, R. Relationships Between the Carbon-Oxygen Stretching Frequencies of Carboxylate Complexes and the

Type of Carboxylate Coordination. *Coord. Chem. Rev.* **1980**, *33* (3), 227–250.

(50) Lan, Y.; Xu, L.; Yan, Y.; Huang, J.; de Keizer, A.; Besseling, N. A.; Stuart, M. A. C. Promoted Formation of Coordination Polyelectrolytes by Layer-by-Layer Assembly. *Soft Matter* **2011**, *7* (7), 3565–3570.

(51) Ornatska, M.; Peleshanko, S.; Rybak, B.; Holzmüller, J.; Tsukruk, V. V. Supramolecular Multiscale Fibers through One-Dimensional Assembly of Dendritic Molecules. *Adv. Mater.* **2004**, *16* (23–24), 2206–2212.

(52) Li, J.; Shi, K.; Drechsler, M.; Tang, B. Z.; Huang, J.; Yan, Y. A Supramolecular Fluorescent Vesicle Based on a Coordinating Aggregation Induced Emission Amphiphile: Insight into the Role of Electrical Charge in Cancer Cell Division. *Chem. Commun. (Cambridge, U. K.)* **2016**, *52* (84), 12466–12469.

(53) Torchilin, V. Tumor Delivery of Macromolecular Drugs Based on the EPR Effect. *Adv. Drug Delivery Rev.* **2011**, *63* (3), 131–135.

(54) Maeda, H.; Sawa, T.; Konno, T. Mechanism of Tumor-Targeted Delivery of Macromolecular Drugs, Including the EPR Effect in Solid Tumor and Clinical Overview of the Prototype Polymeric Drug SMANCS. *J. Controlled Release* **2001**, *74* (1–3), 47–61.

(55) Yang, H.; Chen, Z.; Zhang, L.; Yung, W. Y.; Leung, K. C.; Chan, H. Y.; Choi, C. H. Mechanism for the Cellular Uptake of Targeted Gold Nanorods of Defined Aspect Ratios. *Small* **2016**, *12* (37), 5178–5189.

(56) Lock, L. L.; Reyes, C. D.; Zhang, P.; Cui, H. Tuning Cellular Uptake of Molecular Probes by Rational Design of Their Assembly into Supramolecular Nanoprobes. *J. Am. Chem. Soc.* **2016**, *138* (10), 3533–3540.

(57) Chithrani, B. D.; Ghazani, A. A.; Chan, W. C. Determining the Size and Shape Dependence of Gold Nanoparticle Uptake into Mammalian Cells. *Nano Lett.* **2006**, *6* (4), 662–668.

(58) Cho, E. C.; Zhang, Q.; Xia, Y. The Effect of Sedimentation and Diffusion on Cellular Uptake of Gold Nanoparticles. *Nat. Nanotechnol.* **2011**, *6* (6), 385–391.

(59) Li, J.; Liu, K.; Chen, H.; Li, R.; Drechsler, M.; Bai, F.; Huang, J.; Tang, B. Z.; Yan, Y. Functional Built-In Template Directed Siliceous Fluorescent Supramolecular Vesicles as Diagnostics. *ACS Appl. Mater. Interfaces* **2017**, *9* (26), 21706–21714.

(60) Situ, B.; Chen, S.; Zhao, E.; Leung, C. W. T.; Chen, Y.; Hong, Y.; Lam, J. W. Y.; Wen, Z.; Liu, W.; Zhang, W.; Zheng, L.; Tang, B. Z. Real-Time Imaging of Cell Behaviors in Living Organisms by a Mitochondria-Targeting AIE Fluorogen. *Adv. Funct. Mater.* **2016**, *26* (39), 7132–7138.

(61) Gu, X.; Zhao, E.; Zhao, T.; Kang, M.; Gui, C.; Lam, J. W.; Du, S.; Loy, M. M.; Tang, B. Z. A Mitochondrion-Specific Photoactivatable Fluorescence Turn-On AIE-Based Bioprobe for Localization Super-Resolution Microscope. *Adv. Mater.* **2016**, *28* (25), 5064–5071.